Shakti Spin Ice: investigation of arrays of cobalt rectangular nanoislands

Marta Galbiati*,

Abstract
In this article, the Shakti spin ice will be studied through micromagnetic simulations. Spin ices are arrays of single-domain nanostructures that have revealed peculiar properties and complex behaviours. In this work the basic elements of the Shakti spin ice will be explored from an energetic point of view. Each basic element is a vertex in which four, three or two nanoislands meet. According to the alignments of the magnetic moments of the islands of the vertex, different configurations(types) can be identified, each one with its own energy. A larger portion of the lattice will be then considered. Many equilibrium magnetization configurations are possible in this case and even if a degenerate ground state exist, the one made by lower energy types, it is never reached in simulations. At the end, the application of an external field will be considered. Indeed, it is possible to saturate the structure and to study how the equilibrium magnetization changes after the removal of the field.

***Corresponding author**: marta1.galbiati@mail.polimi.it

Contents

1. Introduction

1.1 Artificial Spin Ice: Shakti structure

Artificial spin ices are arrays of single-domain ferromagnetic nanostructures, designed artificially and placed in close proximity so that the magnetic moment interactions lead to complex correlated behaviour[2]. They were introduced initially to mimic the frustrated behaviour of naturally occurring spin ice materials and to reproduce the famous two-dimensional Ising model.

Frustration has a central role in these system. It emerges from the impossibility of simultaneously minimizing all interactions. In general, frustration can arise from intrinsic structural disorder, as in spin glasses, or in a regular geometry that carefully balances competing interactions(geometrical frustration). Macroscopic entropy even at very low temperatures is a fundamental characteristic of frustrated systems.

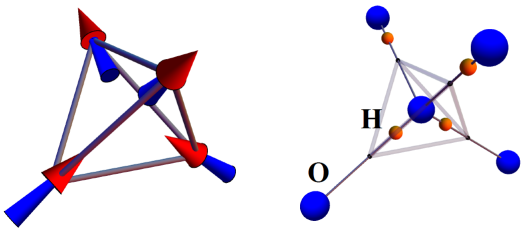

Figure 1. The Ice Rule: in (cubic) water ice (right) and the corresponding spin configuration(left). From [3].

The name spin ice comes from the fact that water ice is one of the first studied examples of these frustrated systems. Pauling explained the measurements of the zero temperature entropy of water in terms of multiple choices in allocating hydrogen bonds between H_2O molecules in ice[3]. A given oxygen atom in water ice is situated at a vertex of a diamond lattice and has four nearest neighbour oxygen atoms(tetrahedral coordination), each connected via an intermediate proton. The proton is not centered between the two surrounding oxygens, but rather is positioned closer to one or the other. The lowest energy state has two protons positioned close to the oxygen and two protons positioned further away, forming a "two-in—two-out" state. Such states are said to obey an ice rule (**Figure 1**). In the early 1990's certain magnetic materials displaying an unusual behaviour were studied. They were characterized by lack of conventional magnetic ordering down to very low temperatures as a consequence of geometrical frustration. Pyrochlore materials, such as $Ho_2Ti_2O_7$, showed the same behaviour, with configurations characterized by spins pointing

toward the center of the tetrahedron or outward. In the ground state the sum of all the spins in a vertex should be zero: two spins pointing out and two pointing into a tetrahedron.
Artificial spin-ice systems have emerged as two dimensional prototypes of these materials. They are typically fabricated using electron beam lithography and can be engineered to study frustrated spin systems, monopole-like excitations and out-of-equilibrium thermodynamics.
Artificial spin ice has primarily been studied in two simple lattice structures: the square lattice, with four-moment coordination at each vertex and the Kagome lattice(also called honeycomb or hexagonal), with three-moment coordination at each vertex. In **Figure 2**, these two geometries are reported. A variant of the Kagome is the brickwork lattice in **Figure 3**. Another artificial spin ice has been introduced later. It allows to design and study a non-trivial frustrated geometry inaccessible in any natural system. Such a geometry was proposed in the form of a 'Shakti' lattice(**Figure 4**). This lattice has mixed coordination: the magnetic moments can meet at vertices of two, three or four, which distinguishes it from any other artificial spin-ice material.

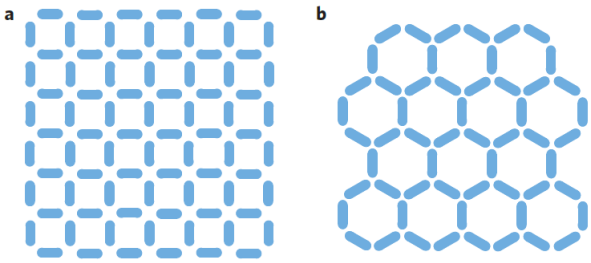

Figure 2. Square(a) and Kagome(b) spin ice geometries. From [2].

Shakti appears as a mixture of square and brickwork basic units. All the structures have as basic element a nanoisland elongated in a certain direction. Because of shape anisotropy magnetic moments prefer to be aligned along that direction. Shakti structure comes from the square lattice removing some nanoislands in order to create a new periodic array.

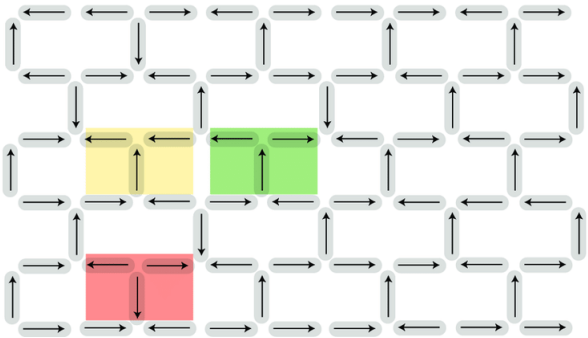

Figure 3. Brickwork spin ice with its possible vertex configurations highlighted: Type1(green), Type2(yellow) and Type3(red).

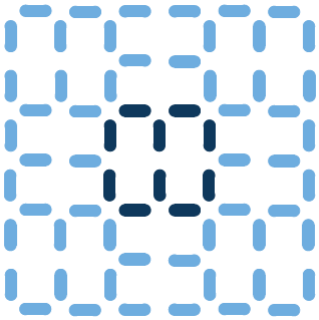

Figure 4. The protagonist of this work: Shakti spin ice. From [2].

Square Spin ice was introduced by Wang et al.[6]. They fabricated it with permalloy, $Ni_{80}Fe_{20}$, characterized by isotropic magnetic properties. If one considers a single vertex of four islands, then the lowest magnetostatic energies states have two magnetic moments oriented in toward the center and two oriented away from the center, in direct analogy to the tetrahedra of spin ice materials. However perpendicular islands interact more than parallel ones so that degeneracy of the ice rule is lifted[4]. This leads to a unique antiferromagnetic ground state, and therefore to an absence of residual entropy. Experimentally the ground state is seen after the application of thermalization protocols to the structure. Wang at al. could not see it because of the AC demagnetization to which the artificial spin ice was subjected.
In the Kagome spin ice each vertex connects three nanoislands and the magnetostatic energy of the vertex is minimized when it obeys a pseudo-ice rule which dictates that two magnetic moments point in and one points out, or viceversa.
The brickwork lattice shares the topology of the honeycomb lattice while, as in square ice, the interactions between spins are not equivalent. From the point of view of pure vertex energy, it possesses a, equivalent to that of the square artificial spin ice.
In conclusion square and brickwork basic units, which compose the Shakti lattice, do not follow the ice rule in normal conditions and they have a unique ground state. However, Shakti lattice shows frustration associated with the lattice topology[2] since there is no way to accomodate the lower energy types in the lattice. This fact distinguishes it from any other artificial spin-ice material studied so far. In experiments, the degenerate ground states is found if a thermalization protocol is applied [2].

1.2 Main objectives

The main scope of this article is the study of the Shakti spin ice through micromagnetic simulations. **First** of all, the basic vertex configurations have been considered. In Shakti lattice the basic elements are the four vertex configuration, the three and the two vertex configurations, then also combinations of them can be considered. They have been studied from the energetic point of view. Investigations of the relations among

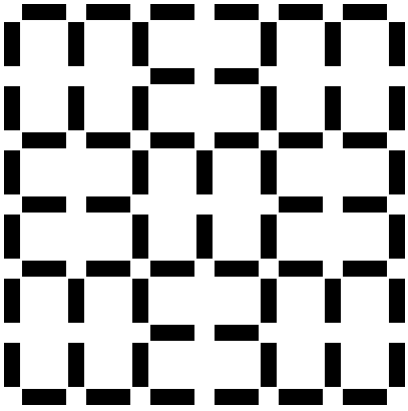

Figure 5. The lattice made of rectangular nanoislands used for most of the simulations($2020 \cdot 2020 pixels$).

the energies of the four vertex units and the type of material, the nanoisland shape and the simulation parameters have revealed complex influences on the simulation results.
The **second** instance addressed was the analysis of the possible configurations of a portion of the lattice **Figure 5**. In this context, the frequency of occurrence of the basic elements has been studied and it has been correlated with the multiplicity of each unit rather than with its energy.
Finally, the effect of the application of a magnetic field has been considered in order to calculate the hysteresis loop for the portion of lattice.
In the majority of the simulations of this article the material considered for the nanoislands is polycrystalline cobalt and the shape considered is rectangular. Both these features are unusual with respect to experiments and simulations presented in literature, in which the most used material is permalloy and the shape of the nanoisland is curved as in the figures above.

1.3 Methodology for simulations

Micromagnetic simulations have been realized with OOMMF [1]. The value used for damping coefficient α in the RungeKutta evolver is 0.5. The TimeDriver stops when the the maximum change dM/dt of any spin being simulated falls below the value 0.1. These are standard values, in general good to get not too slow convergence of the algorithm. The material is inserted in the simulation through its exchange constant, $A = 31 \cdot 10^{-11} \frac{J}{m}$ for cobalt and $\frac{J}{m} A = 10 \cdot 10^{-11} \frac{J}{m}$ for permalloy, and through its saturation magnetization, $Ms = 1.44 \cdot 10^6 \frac{A}{m^2}$ for cobalt and $Ms = 8.4 \cdot 10^5 \frac{A}{m^2}$ for permalloy. In each simulation a correct dimension for the cell must be imposed. The following formula allows to estimate the correct cell dimension since it must be $\leq \lambda_{ex}$.

$$\lambda_{ex} = \sqrt{\frac{2A}{\mu_0 Ms^2}} \tag{1}$$

$$\lambda_{ex} = 4.8778\, nm\, for\, cobalt \tag{2}$$

$$\lambda_{ex} = 4.7493\, nm\, for\, permalloy. \tag{3}$$

In the first part, the simulations of vertex configurations are carried out with $cell\ size = 4\,nm$ or $cell\ size = 5\,nm$ in every direction, choices compatible with the above requirement, while the overall space of simulation is around $500\,nm \cdot 500\,nm$. In the next parts it is necessary to increase the cell to simulate over spaces larger than $1500\,nm \cdot 1500\,nm$, corresponding to a portion of the lattice. Furthermore, in this case the problem of vortices occurs: some islands do not show a single-domain behavior, they are not compatible with the spin-ice system that is being simulated. Increasing the exchange constant has proved to be a solution to this problem, therefore, the first possible values of A that avoid the vortices have been used , fixing the cell at $10\,nm$. The higher exchange constant increases the λ_{ex}, allowing to obtain a consistent simulation. Furthermore the interactions between the islands that are crucial for determining the conconfigurations of the spin ice are essentially dipolar[5] allowing for changing the exchange constant without many concerns. Note that in the first part, where the type of material is an important parameter, the exchange constant is not changed.

Figure 6. Four island vertex with curved features, used for a comparison between rectangular and curved shape. From [5].

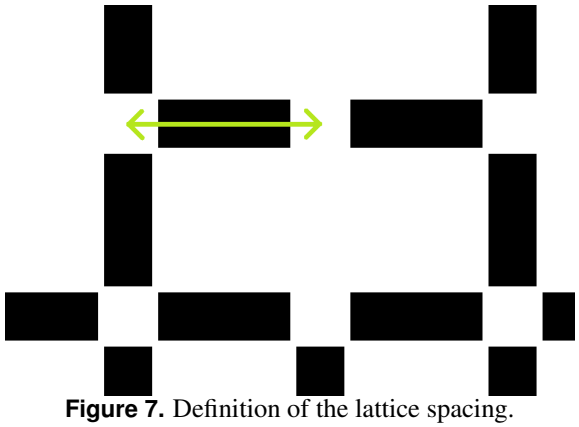

Figure 7. Definition of the lattice spacing.

1.4 Shape definition

In OOMMF simulations it is possible to insert complex geometries through images. For this work two images have been used. One has curved nanoislands, it is the same used in [5] and is reported in **Figure 6**. It will be used for the

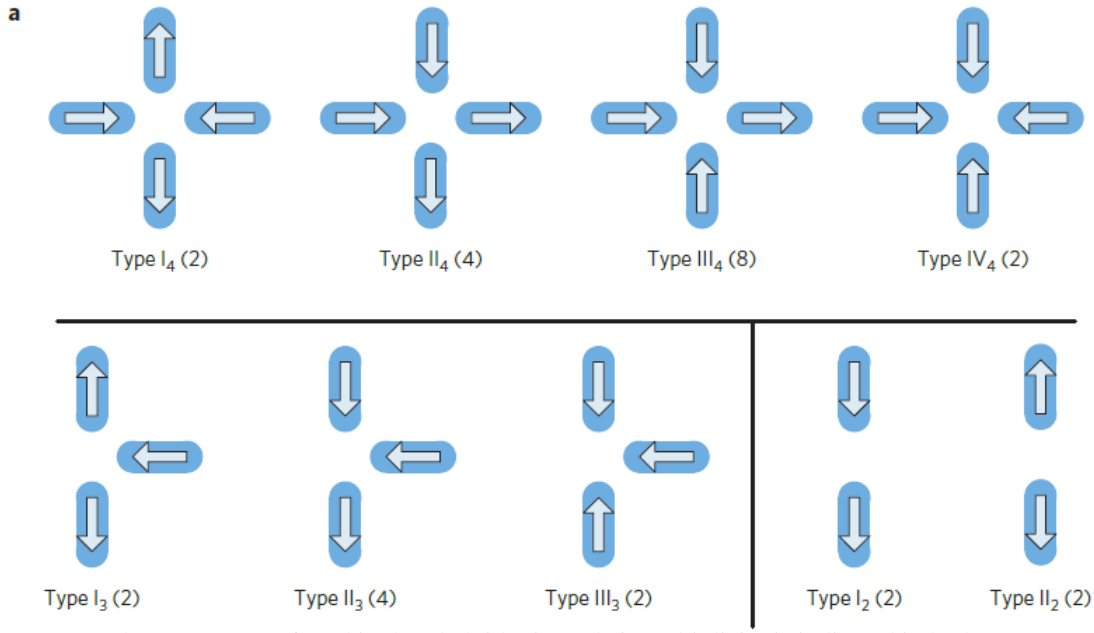

Figure 8. The vertex types found in the Shakti lattice. Their multiplicity is indicated in brakets. From [2].

simulations of the four vertex configurations in order to understand the dependence of the vertex energy on the shape. The other image used is **Figure 5**, or a part of it, and is constructed with pixel precision($2020 \cdot 2020 pixels$): each island measures $220 \cdot 80 pixels$ and the distances among them are of $50 pixels$. The use of an image with pixel precision allows to better control the geometry definition and the relation with the nanometric dimensions. These dimensions are the same of [2] and in general are among the commonest in literature. With a direct equivalence from pixel to nanometers the lattice with $spacing = 320\,nm$ is obtained. See **Figure 7** for the definition of spacing. Other spacings used are $spacing = 160\,nm$ and $spacing = 240\,nm$, the latter does not correspond to an integer value of pixels. Also the lattice with $spacing = 320\,nm$ has been considered, but concerns have arisen in simulations of a so large space avoiding vortices, so it will not be considered.

2. Simulation results discussion

2.1 Vertex energies

In the Shakti spin ice three basic elements are present and they are reported in **Figure 8**. For the **four-island vertex** there are 16 ways of placing magnetic moments on the single-domain islands but many of them are practically identical, therefore it is possible to consider four types: two-in-two-out with favoured perpendicular interaction(type1), two-in-two-out with favoured parallel interaction(type2), three-in-one-out(type3) and all-in(type4). The total energy, magnetostatic plus exchange energy, is the interesting parameter of different magnetic vertex configurations. In the article [5], the relative energies of the different four configurations have been analysed as a function of some geometrical parameters, like the gap between neighbouring nanomagnets, the thickness of the nanomagnets and the aspect ratio(length divided by the width of the nanoisland). No strong changes appear in the distribution of energies changing these parameters. In the following, what happens to relative energies changing the shape, the material and the cell size is analysed. The definition of relative energy is:

$$E_i = \frac{e_i - e_1}{e_4 - e_1} \tag{4}$$

with e_1 and e_4 the energies of the types with lower energy and higher energy respectively. To test the shape dependence, the same image of [5] have been used to allow a comparison, while, to test the material dependence, permalloy and cobalt were considered. Finally the cell size considered was $5\,nm$ in one case and $4\,nm$ in all the other cases. The island dimensions for curved and rectangular shape are similar, indeed the overall vertex dimensions are $500\,nm \cdot 500\,nm$ and $540\,nm \cdot 540\,nm$. The simulations were carried out imposing the magnetization of the possible configurations and then letting the system relax, it obviously remains in the same configuration reaching equilibrium. It must be reported that the system, starting from casual magnetization, does not reach the configuration of minimum energy, but it can populate different available configurations. The results of the relative energies are reported in **Figure 9**. A precise pattern cannot be identified. The results seem to depend on all the three parameters and not independently since, fixing the cell dimension to $4\,nm$, the curved shape is more affected by the type of material than the rectangular one which shows practically the same behavior. But things are different if the cell is changed: the rectangular shape in cobalt at $5\,nm$ gives a different distribution with respect to the analogous case at $4\,nm$. Furthermore, in two cases type1 and type 2 are almost degenerate with respect

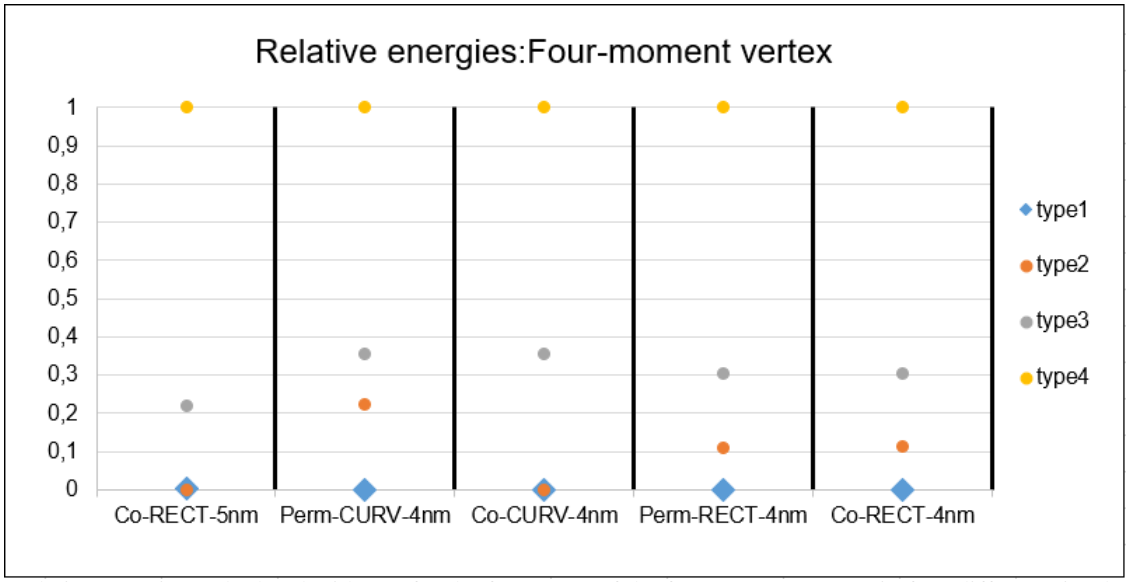

Figure 9. Relative energies, calculated with (4), for the four types of the four-moment vertex in four different simulations with: rectangular island made of cobalt with cell size of $5\,nm$, curved island made of permalloy with cell size of $4\,nm$, curved island made of cobalt with cell size of $4\,nm$, rectangular island made of permalloy with cell size of $4\,nm$ and finally rectangular island made of cobalt with cell size of $4\,nm$.

to the other cases. The behavior appears very complex and maybe much more simulations could help to understand it better. For the curved shape in permalloy the results are consistent with [5]. The rectangular shape gives in general more similar values for the energies of the first three types. This can be understood in relation to the results of [5], the rectangular shape is characterized by a smaller gap between neighbouring nanomagnets and by an higher aspect ratio, both these cases lead to lower energies for the first three types. The analysis of the absolute energies(**Figure 10**) in the five cases gives further information. The energies of the rectangular shaped vertices are higher than the curved ones, this because of the edges of the rectangles. Indeed, in the edges of the rectangular islands, magnetic moments are usually not aligned in the direction imposed by shape anisotropy causing an increase of energy. Cobalt-made vertices are more energetic than permalloy ones because of their intrinsic properties, e.g. higher exchange interaction. The nearly degeneracy in energy of type1 and type2 is stronger in the curved shape at $4\,nm$ with respect to rectangular shape at $5\,nm$. Surprisingly in both cases type2 has lower energy than type1! But from these simulations is impossible to explain it, because this result cannot be easily correlated with one of the changed parameters.

Having in mind the complexity of the results obtained, the **three-island vertex** is now analysed in the case of rectangular-shaped nanoislands made of cobalt, with dimensions $320\,nm \cdot 80\,nm$. The possible configurations are eight but some of them are identical, hence three different types are usually considered. Simulations with cell size of both $4\,nm$ and $5\,nm$ have been carried out. As before the relative energies and the absolute ones are considered for the different types. The strong effect of the cell size still emerges: the absolute ener-

Co-RECT-5nm		Perm-RECT-4nm	
Type	Total Energy(10^-17 J)	Type	Total Energy(10^-17 J)
1	3,442798	1	2,384813
2	3,440685	2	2,477712
3	3,694204	3	2,641000
4	4,590259	4	3,229020
Perm-CURV-4nm		**Co-RECT-4nm**	
Type	Total Energy(10^-18 J)	Type	Total Energy(10^-17 J)
1	3,013282	1	7,045744
2	3,102648	2	7,323679
3	3,154679	3	7,803971
4	3,412691	4	9,537816
Co-CURV-4nm			
Type	Total Energy(10^-18 J)		
1	8,860173		
2	8,860173		
3	9,275712		
4	10,034065		

Figure 10. Absolute energies for the four types of the four-island vertex in five different simulations with: rectangular island made of cobalt with cell size of $5\,nm$, curved island made of permalloy with cell size of $4\,nm$, curved island made of cobalt with cell size of $4\,nm$, rectangular island made of permalloy with cell size of $4\,nm$ and finally rectangular island made of cobalt with cell size of $4\,nm$.

Co-RECT-4nm		Co-RECT-5nm	
Type	Total Energy(10^-17 J)	Type	Total Energy(10^-17 J)
1	5,462036	1	2,586105
2a	5,668519	2	2,655417
2b	5,708051	3	3,103543
3	6,653641		

Figure 11. Absolute energies for the types of the three-moment vertex in two different simulations with: rectangular islands with dimensions $320\,nm \cdot 80\,nm$, made of cobalt and with cell size of $4\,nm$ and of $5\,nm$.

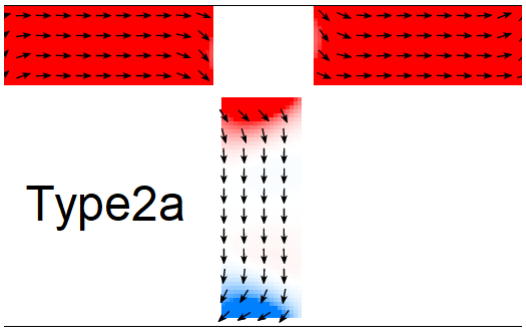

Figure 12. Type2a, a configuration of the three-moment vertex that emerges with a proper energy and degeneracy 2 when simulating rectangular shaped nanoislands with dimensions $320\,nm \cdot 80\,nm$, made of cobalt and with cell size of $4\,nm$.

gies(**Figure 11**) are of the same order of magnitude but, as in the previous case, they increase lowering the cell size. Furthermore, with cell size of $4\,nm$, type 2 gives rise to two different two-fold degenerate types: type2a and type 2b showed in **Figure 12** and **Figure 13**. The splitting of the type2 vertex in two possible alternatives is seen also in the distribution of relative energies(**Figure 14**), together with an increase of the average energy of the two types with respect to the single type2 simulated with cell size of $5\,nm$. Type1 and type2 are not degenerate, as already known for the brickwork lattice. Type1 is favoured because it better accommodates the interactions between perpendicular islands.

The last and simplest basic unit is the **two-moment vertex**. It has 4 possible configurations two by two identical, therefore we can consider two types: type1, with magnetic moments aligned, and type2, with opposite magnetic moments. This case is not so much interesting and only the absolute energies(**Figure15**) are considered, in a single simulation with cobalt-made nanoislands, with dimensions $320\,nm \cdot 80\,nm$ and with cell size of $4\,nm$. Obviously the case with aligned magnetic moments shows a lower energy.

Combinations of the previous units can be considered. One of them, made of six islands, is very interesting and is showed in figure **Figure 16**. With this **6-island geometry** you can cover the entire lattice with no overlap by rotating it of 90^o at each step. It is a combination of two three-island vertices and one two-island vertex, therefore all its 64 possible configurations

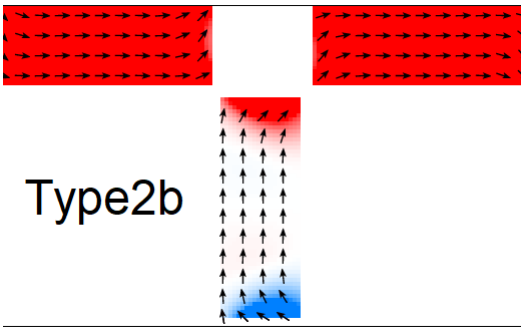

Figure 13. Type2a, a configuration of the three-moment vertex that emerges with a proper energy and degeneracy 2 when simulating rectangular shaped nanoislands with dimensions $320\,nm \cdot 80\,nm$, made of cobalt and with cell size of $4\,nm$.

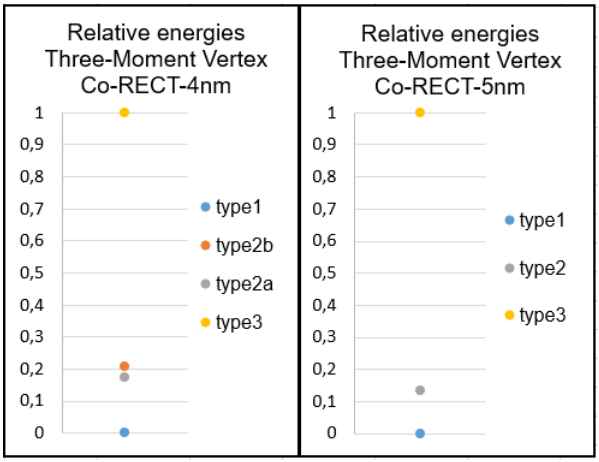

Figure 14. Relative energies, calculated with (4), for the types of the three-moment vertex in two different simulations with: rectangular islands made of cobalt, with dimensions $320\,nm \cdot 80\,nm$ and with cell size of $4\,nm$ and of $5\,nm$.

can be classified according to the possible combinations of these three vertices. 64 simulations were performed imposing the initial configuration. Rectangular-shaped nanoisland with dimensions $320\,nm \cdot 80\,nm$, made of cobalt were simulated with a cell size of $5\,nm$. Twelve possible types emerge for this geometry, they are reported in **Figure 17** with their relative energies calculated with (4). In the figure the types are indicated through the basic elements forming them, also their degeneracies are indicated. The basic elements determine the energy of a configuration: combinations of types with lower energies bring to lower overall energies like the combination of two type1 for the three-island vertices and type1 for the two-island vertex. Note that it is more important to minimize the energy of the two-island vertex, to which an higher absolute energy is associated (**Figure 15**), rather than minimizing the three-island vertices, characterized by lower absolute energies(**Figure 15** with cell size of $5\,nm$). In accordance with what has been said before, with a cell size

Co-RECT-4nm	
Type	Total Energy(10^-17 J)
1	3,995614
2	4,317208

Figure 15. Absolute energies for the two types of the two-moment vertex in a simulation with rectangular islands with dimensions $320\,nm \cdot 80\,nm$, made of cobalt and with cell size of $4\,nm$.

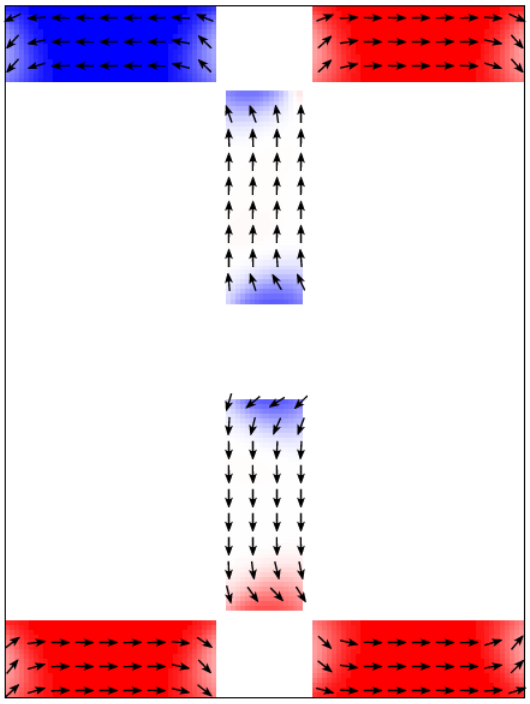

Figure 16. One of the possible configurations of the 6-island geometry. The dimensions of each island are $320\,nm \cdot 80\,nm$. Simulated with the parameters of cobalt with cell size of $5\,nm$.

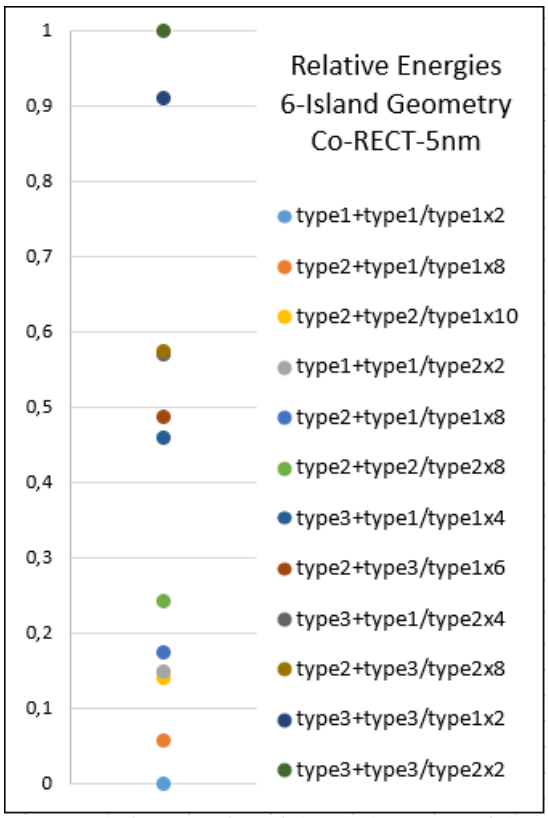

Figure 17. Relative energies of the twelve types of the 6-island geometry calculated with (4). The configurations are indicated through this notation: (type of one three-moment vertex) + (type of the other three moment vertex) / (degeneracy of the configuration). Simulations were carried out on rectangular islands with dimensions $320\,nm \cdot 80\,nm$, made of cobalt and with cell size of $5\,nm$.

of $5\,nm$ there is no splitting of the type2 of the three-moment vertex in two alternatives with different energies. However, some anomalies have been found and two of the reported data are average energies of two very similar configurations. The absolute energies of the twelve types identified are reported in **Figure 18**.

2.2 Lattice configurations and vertex frequency

Now, the results of the simulations executed on the portion of lattice reported in **Figure 5** will be explained. The problem of vortices arises(**Figure 19**) when a large number of islands is considered, when the cell size is increased for computational reasons and when the spacing of the lattice increases. As already explained before, to avoid this problem the exchange constant has been increased. The selected value of the exchange constant is the smallest one that allows to eliminate all vortices. The lattice of dimensions $4040\,nm \cdot 4040\,nm$ has not been considered because a too high value of exchange constant was needed to avoid vortices. Indeed, when the islands become too large, single domain behaviour is not granted and complex dynamics can occur on the single island **Figure 19**.

Co-RECT-5nm
Total Energy(10^-17 J)
5,084440
5,151703
5,250521
5,259556
5,290266
5,370337
5,625055
5,656138
5,753888
5,759753
6,154867
6,259028

Figure 18. Absolute energies of the twelve types of the 6-island geometry. The colors correspond to the ones used in **Figure 17**. Simulations were carried out on rectangular islands with dimensions $320\,nm \cdot 80\,nm$, made of cobalt and with cell size of $5\,nm$.

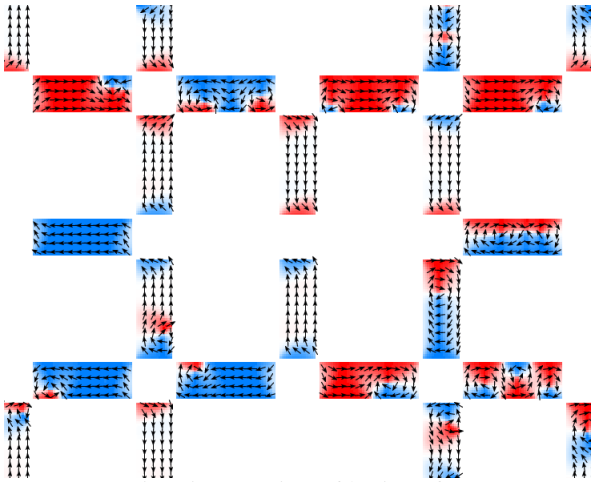

Figure 19. Vortices in a portion of lattice of $4040\,nm \cdot 4040\,nm$ simulated with cell size of $10\,nm$, islands made of cobalt.

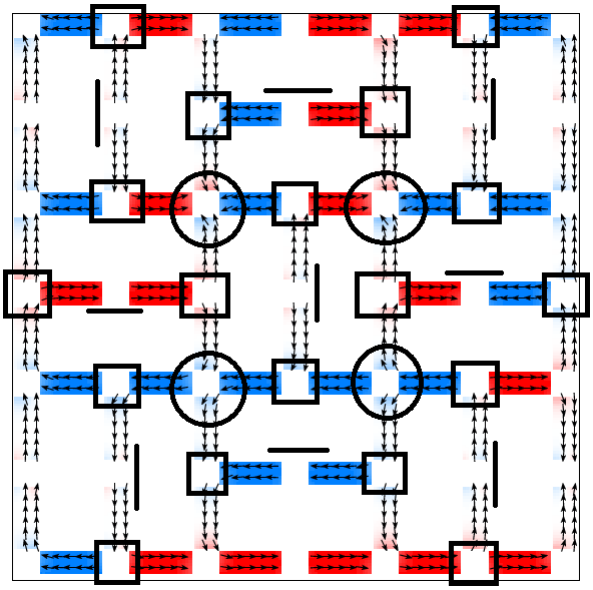

Figure 20. Possible output of the $2020\,nm \cdot 2020\,nm$ lattice simulation with the vertices considered for the study of frequencies. 4 four-moment vertices(circles), 18 three-moment vertices(squares) and 9 two-moment vertices(lines).

The following sets of simulations with rectangular islands made of cobalt have been performed:

- $1010\,nm \cdot 1010\,nm$ lattice(2 pixels per nm), lattice spacing of $160\,nm$, exchange constant $A = 40 \cdot 10^{-11}\ \frac{J}{m}$ and cell size $5\,nm$.
- $1520\,nm \cdot 1520\,nm$ lattice(~ 1.3 pixels per nm), lattice spacing of $\sim 240\,nm$ and exchange constant $A = 100 \cdot 10^{-11}\ \frac{J}{m}$ and cell size $10\,nm$.
- $2020\,nm \cdot 2020\,nm$ lattice(1 pixel per nm), lattice spacing of $320\,nm$, exchange constant $A = 110 \cdot 10^{-11}\ \frac{J}{m}$ and cell size $10\,nm$.

For each lattice dimension, 10 simulations have been performed starting from random magnetization.
The final total energies and magnetization configurations have been studied. The number of possible configurations of the lattice is very high: 2^{66}. For each simulation the vertices showed in **Figure 20** have been considered in order to study the frequencies of occurrence of the different types for the four-moment, three-moment and two-moment vertices. The 6-island geometry was not considered since, as explained before, it is simply a combination of the more fundamental vertices. The results for the frequencies of occurrence are reported in **Figure 21**, **Figure 22** and **Figure 23**. The values are normalized with respect to the total number of vertices. The four-moment vertex frequency can be considered anomalous because of the low number of these vertices present in the portion of lattice considered. However, it is clear that the system does not prefer the types with lower energies but

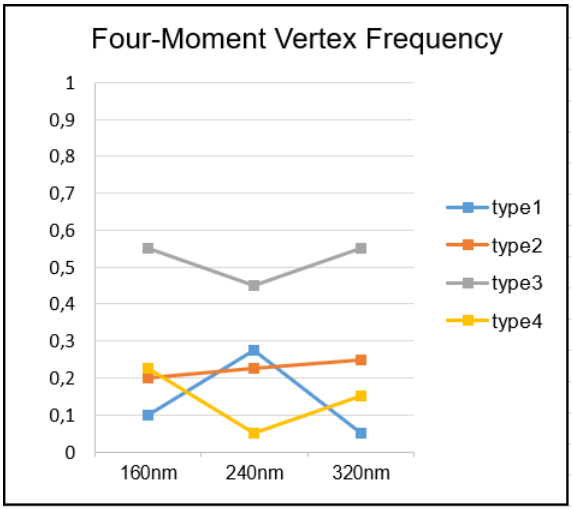

Figure 21. Frequency of occurrence of the four types of the four-moment vertex for different values of the lattice spacings, 160 nm, 240 nm and 320 nm. The values are normalized with respect to the total number of vertices, 4.

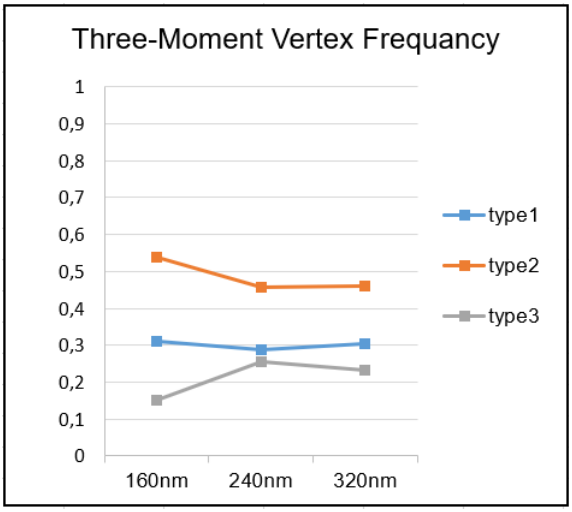

Figure 22. Frequency of occurrence of the three types of the three-moment vertex for different values of the lattice spacings, 160 nm, 240 nm and 320 nm. The values are normalized with respect to the total number of vertices, 18.

rather those with higher degeneracy. The fractions associated to the degeneracy of each type, for a given vertex, are reported in **Figure 24** and the fractions coming from simulations are quite in agreement with them, except for few anomalies.

The results obtained are in contrast with what is obtained from experiments, for example in [2] exactly the same study is performed. For the values of spacings considered here, experiments give frequencies directly related to the energies of the different types, so that the most frequent types are those with lower energies, only with lattice spacings larger than 800 nm the fractions of types correspond to those given by their degeneracies. While in the experiments thermalization protocols are executed in order to reach the degenerate ground state of the structure, in simulations it is not possible to reach the true minimum of energy for each type and a random distribution prevails.

The average energies for the three sets of simulations are:

- $1010\,nm \cdot 1010\,nm$ lattice $\rightarrow 2,535235 \cdot 10^{-16}\,J$
- $1520\,nm \cdot 1520\,nm$ lattice $\rightarrow 4,520337 \cdot 10^{-16}\,J$
- $2020\,nm \cdot 2020\,nm$ lattice $\rightarrow 6,577652 \cdot 10^{-16}\,J$.

The Shakti-lattice degenerate ground state, however, exists: it corresponds to all the four-island vertices having a type1 configuration, and the three-island vertices evenly divided between the lowest-energy type1 magnetic island configuration and the type2 magnetic moment configurations as required by the lattice topology[2]. Degeneracy arises from the different possible ways of placing type1 and type2 on the three moment vertices. A possible ground state has been simulated for $2020\,nm \cdot 2020\,nm$ lattice imposing its magnetization from the beginning and it is represented in **Figure 25**. It has an energy of $5,881012 \cdot 10^{-16}\,J$ effectively lower with respect to the average energy found in previous simulations.

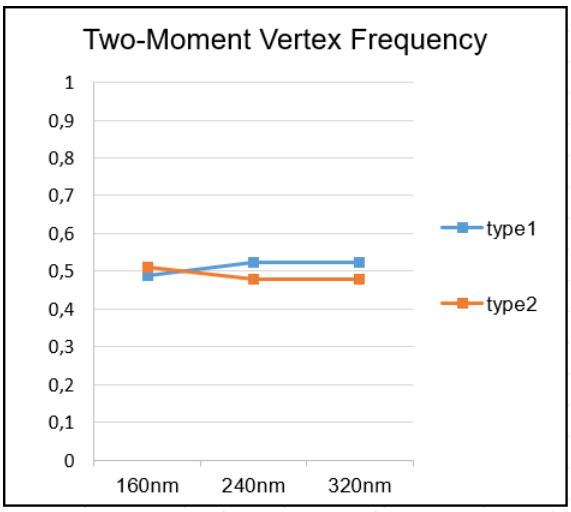

Figure 23. Frequency of occurrence of the two types of the two-moment vertex for different values of the lattice spacings, 160 nm, 240 nm and 320 nm. The values are normalized with respect to the total number of vertices, 9.

Four-moment vertex		Three-moment vertex	
Type	Degeneracy Frequency	Type	Degeneracy Frequency
1	0,125	1	0,25
2	0,25	2	0,5
3	0,5	3	0,25
4	0,125	Two-moment vertex	
		Type	Degeneracy Frequency
		1	0,5
		2	0,5

Figure 24. Frequency of occurrence associated to the degeneracy of each type, for a four-moment, three-moment and two-moment vertex.

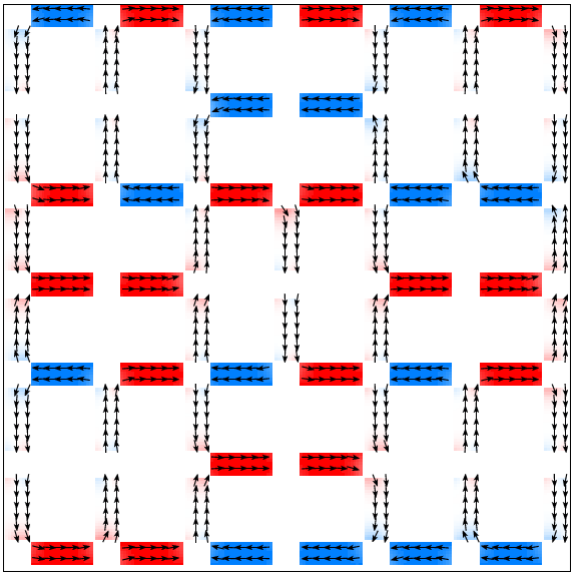

Figure 25. Possible ground state configuration of the $2020\,nm \cdot 2020\,nm$ lattice with types of lower energies, $Total\,Energy = 5,881012 \cdot 10^{-16}\,J$.

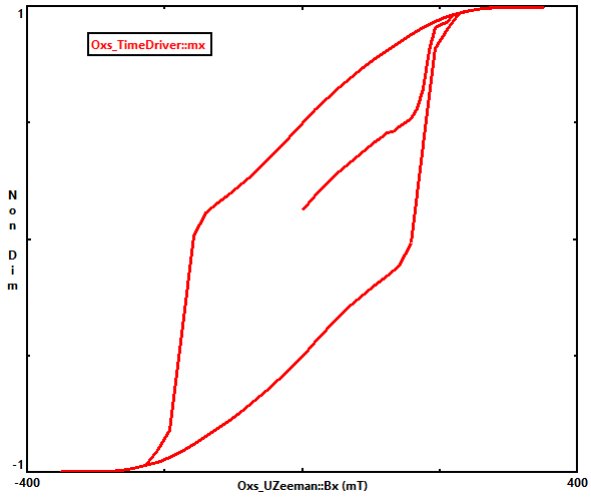

Figure 26. Hysteresis loop for the $(1010\,nm \cdot 1010\,nm)$ lattice, cell size of $10\,nm$, the applied H field is changed from $-3500\,Oe$ to $3500\,Oe$ in 80 stages.

2.3 Behaviour in presence of a magnetic field

The effect of a magnetic field applied along the x direction has been considered on the $(1010\,nm \cdot 1010\,nm)$ lattice, this time simulated with cell size of $10\,nm$ in order to have reasonable times for the simulations of all the stages required. The exchange constant has been increased to $A = 100 \cdot 10^{-11}\ \frac{J}{m}$ to avoid vortices. The starting point for the simulation was a magnetization configuration obtained for the same lattice starting from random magnetization. The applied H field is changed from $-3500\,Oe$ to $3500\,Oe$ in 80 stages. The hysteresis loop in **Figure 26** is obtained. With an applied field of nearly $3230\,Oe$, the saturation of the structure is obtained. It is interesting to study what happens after the application of the saturation field. Considering the same lattice, starting with random magnetization, the system is brought to saturation in the x direction, then the field is removed in one stage. The simulation was repeated 5 times and the same configuration was reached in all the cases(**Figure 27**). All the islands parallel to the x direction remain in the saturation configuration pointing towards right because after the removal of the field they are fixed in that direction by their shape anisotropy and there is no way to have a spontaneous magnetic momentum reversal. While the islands perpendicular to the x direction , after the removal of the field, are driven by their shape anisotropy to point in the vertical direction, up or down. During the relaxation of these islands they are affected strongly by the other perpendicular islands and the equilibrium configuration obtained is always the same with $Total\,Energy = 2,614302 \cdot 10^{-16}\,J$.

The vertex frequencies in this final configuration are obviously different with respect to the case in which a field is not applied. The comparisons between field and no field case are showed in **Figure 28**, **Figure 29** and **Figure 30**. The

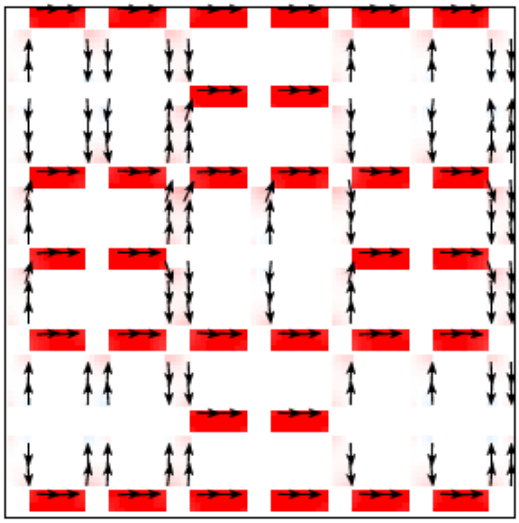

Figure 27. Final configuration for the $(1010\,nm \cdot 1010\,nm)$ lattice, cell size of $10\,nm$, after the application of the saturation field. All the horizontal island point in the direction of the applied field.

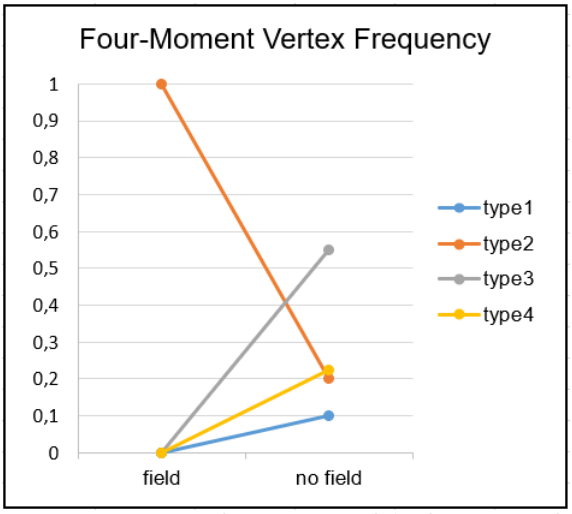

Figure 28. Frequency of occurrence of the four types of the four-moment vertex after the application of the saturation field and its removal(field) and without the application of any field (no field), for the $(1010\,nm \cdot 1010\,nm)$ lattice, cell size of $10\,nm$.

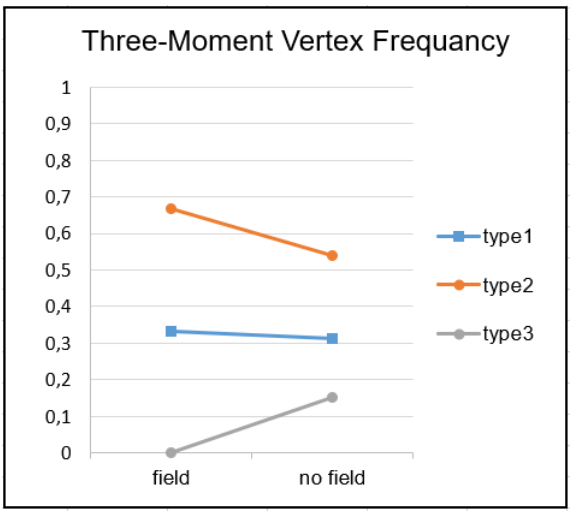

Figure 29. Frequency of occurrence of the three types of the three-moment vertex after the application of the saturation field and its removal(field) and without the application of any field (no field), for the $(1010\,nm \cdot 1010\,nm)$ lattice, cell size of $10\,nm$.

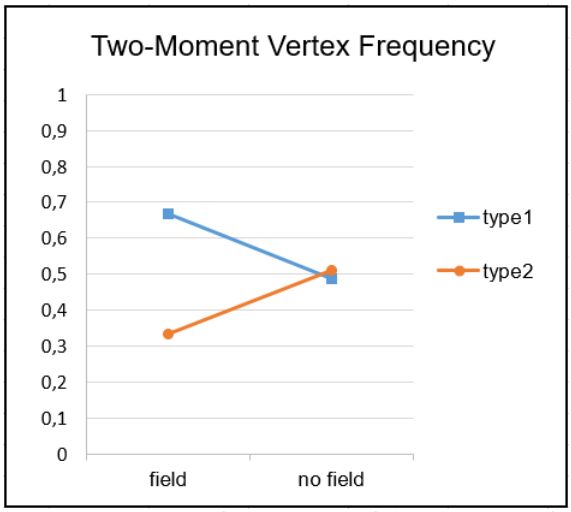

Figure 30. Frequency of occurrence of the two types of the two-moment vertex after the application of the saturation field and its removal(field) and without the application of any field (no field), for the $(1010\,nm \cdot 1010\,nm)$ lattice, cell size of $10\,nm$.

four four-moment vertices have all type2 configurations, the one that with lower energy accommodates the horizontal islands with same magnetic moment direction. Considering the three-moment vertices, type2, characterized by two horizontal islands pointing toward right, becomes much more abundant and finally, for the two-moment vertices, type1 is favoured for the same reasons.

3. Conclusions

In this work Shakti spin ice has been analysed through OOMMF simulations. The simulations were focused on arrays of cobalt-made rectangular nanoislands, however permalloy-made nanoislands and curved shape have been discussed for the four-island vertex underlining complexity related to the dependences of simulation results on parameters like the type of material, the shape of the nanoisland and the cell size for the simulation. A more systematic approach with much more simulations for the different values of that parameters could help to understand the exact dependences. Apart for few anomalies, the analysis of the different types of vertices of the Shakti spin ice have produced results coherent with the literature. Combinations of the usual vertices can be used for the study of the lattice, as seen in the 6-island geometry.
Then the possible configurations of a portion of Shakti spin ice have been considered. The system simulated does not reach its degenerate ground state but generally falls into arbitrary configurations, showing all type of vertices with fractions related to their multiplicity. Further studies could be investigated more about the impossibility to arrive to the degenerate ground state, the same found in experiments after thermalization. This sets a serious limit to the possibility to use

micromagnetic algorithms to simulate experimental results. A possibility could be the implementation of a simulation protocol that allows the system to overcome the energy barriers of the configuration, in which the systems has fallen, and to reach one of the possible ground states. This does not seem to be an easy task because of the very high number of possible configurations for the portion of lattice considered.
Finally the effect of the application of an external field has been considered. It is possible to saturate the structure in one direction and, after the removal of the field, a specific configuration seems to be clearly favoured. Much more simulations could verify these results. It could be interesting to test the application of the field in directions not parallel to any group of islands. In conclusion, the use of micromagnetic simulations for the Shakti spin ice could be further explored unrevealing new emergent complexities and explaining those already discovered.

References

[1] M.J. Donahue and D.G. Porter. "OOMMF User's Guide, Version 1.0". In: *Interagency Report NISTIR 6376* (1999).

[2] Ian Gilbert et al. "Emergent ice rule and magnetic charge screening from vertex frustration in artificial spin ice". In: *Nat Phys* 10 (Sept. 2014), pp. 670–675. DOI: 10.1038/nphys3037.

[3] Cristiano Nisoli, Roderich Moessner, and Peter Schiffer. "Colloquium: Artificial spin ice: Designing and imaging magnetic frustration". In: *Rev. Mod. Phys.* 85 (4 2013), pp. 1473–1490. DOI: 10.1103/RevModPhys.85.1473. URL: https://link.aps.org/doi/10.1103/RevModPhys.85.1473.

[4] Cristiano Nisoli et al. "Ground State Lost but Degeneracy Found: The Effective Thermodynamics of Artificial Spin Ice". In: *Phys. Rev. Lett.* 98 (21 2007), p. 217203. DOI: 10.1103/PhysRevLett.98.217203. URL: https://link.aps.org/doi/10.1103/PhysRevLett.98.217203.

[5] Yann Perrin, Benjamin Canals, and Nicolas Rougemaille. "Vertex micromagnetic energy in artificial square ice". In: (Jan. 2016). DOI: 10.1117/12.2238580.

[6] Ruifang Wang et al. "Artificial 'Spin Ice' in a Geometrically Frustrated Lattice of Nanoscale Ferromagnetic Islands". In: *Nature* 439 (Feb. 2006), pp. 303–6. DOI: 10.1038/nature04447.